Journal of Building Engineering 124 (2026) 116033

Contents lists available at ScienceDirect

Journal of Building Engineering

journal homepage: www.elsevier.com/locate/jobe

Large-scale experimental study of thermal performance of building-integrated photovoltaic façade in an enclosure fire

Chengming Xiao [a], Rui Zhou [a], Dezhi Ran [a], Fengqi Wang [a], Haonan Chen [a], Chiara Bedon [b], Jinhua Sun [a], Yu Wang [a,*]

[a] State Key Laboratory of Fire Science, University of Science and Technology of China, Hefei, 230026, PR China
[b] Department of Engineering and Architecture, University of Trieste, Trieste, Italy

ARTICLE INFO

Keywords:
BIPV façade
Compartment fire
Thermal breakage and fallout
Interaction between PV panels and compartment fire dynamics

ABSTRACT

Building-Integrated Photovoltaic (BIPV) façades play a significant role in enhancing the renewable energy performance and sustainability of modern buildings. However, fire incidents are becoming increasingly common in BIPV systems, yet little is known about the fire performance of BIPV façade. In this work, a total of 16 large-scale fire tests were conducted to investigate the thermal breakage and fallout of BIPV façade in a compartment fire, with a dimension of 1400 × 1400 × 1800 mm^3. Cadmium telluride and monocrystalline silicon BIPV curtain wall components were selected for this study, with traditional glass included for comparison. Significant differences were observed between PV façade and traditional glass façade, with the former exhibiting self-sustained burning, even after the fire extinction. The types of PV panels significantly impact the breakage and fallout times and behavior, as the new openings caused by PV panel fallout alter the stable ventilation condition and induce more flame ejection, resulting in a significant heat flux compared to control cases without samples. Among the tested configurations, double-glazed PV panels with tempered glass demonstrated the best fire performance and are therefore recommended for BIPV façade design. The experimental results would provide important references for the fire safety design of emerging BIPV high-rise buildings.

1. Introduction

With the growing global energy consumption and the increasing concerns over environmental sustainability, improving building energy efficiency and integrating renewable energy sources have gained much interest. Building-integrated photovoltaics (BIPV), which combine energy generation with architectural functionality, have emerged as a promising solution for sustainable urban development, with many new and innovative products over the last few years [1]. According to a recent industry report [2], the worldwide BIPV market is anticipated to expand from USD 39.00 billion in 2026 to USD 123.61 billion by 2033, with a compound annual growth rate of 17.9%. Among all potential installation locations, the building façade is widely recognized as the preferred choice for the installation of BIPV systems [3]. A notable example is the Qingdao Teraeder Headquarter [4], known as the world's first "zero-carbon building". By adopting BIPV glass curtain walls on the east, west, and south façades, the project has achieved 100% replacement with renewable electricity. In addition, several representative BIPV curtain wall projects are currently under development, including the 1428 Brickell skyscraper [5] in the United States and DC Tower 2 [6] in Austria (Europe's first photovoltaic

* Corresponding author.
E-mail address: yuwang@ustc.edu.cn (Y. Wang).

https://doi.org/10.1016/j.jobe.2026.116033
Received 19 December 2025; Received in revised form 25 March 2026; Accepted 3 April 2026
Available online 5 April 2026

façade).

Beyond energy production, integrating PV modules into the building façade enhances architectural aesthetics compared with traditional curtain walls. The realization of these multifunctional and aesthetic advantages is closely linked to PV panel technologies, which can be divided into crystalline silicon (c-Si) and thin-film panels. In the early development of BIPV façade, double-glazed and single-glass crystalline silicon modules were predominantly used due to their high conversion efficiency and long operational lifespan. However, c-Si modules are offering restricted color options and low transparency, which constrains their integration with diverse architectural façades. In recent years, thin-film photovoltaic technology has been widely applied in BIPV due to its excellent low-light performance (high power generation efficiency under weak light conditions) [7]. Moreover, they offer a wide range of colors, adjustable transparency, and flexible module formats, enabling greater architectural customization (Fig. 1(a)).

However, BIPV systems may also pose great fire safety challenges. In recent years, fires involving building photovoltaic systems have been reported worldwide, resulting in severe personal injury and property damage. In the United Kingdom, data showed that photovoltaic fire accidents in 2023 were six times higher than they were ten years prior [12]. The recent fire in an office building in the center of Brussels highlighted this risk [13], as PV panels ignited the building's façade. BIPV façade shares many of the same characteristics as other modern façade systems. The tragic lessons of the Grenfell Tower fire highlighted this risk, as façade fire could spread rapidly across large portions of a building within a short period of time [14]. Typically, BIPV modules consist of fragile glass materials as well as combustible components such as poly-vinyl butyral (PVB) film or ethylene vinyl acetate (EVA), which serves as an encapsulant material in photovoltaic systems. In addition, combustible material Tedlar–Polyester–Tedlar (TPT) is commonly employed as a backsheet for single-layer PV panels, as shown in Fig. 1(c). Under fire conditions, photovoltaic curtain walls may exhibit a three-dimensional fire spread in both horizontal and vertical directions, which further increases the complexity of BIPV façade systems. On the one hand, the combustible materials within PV modules provide additional fire loads to the building, and once ignited, the adjacent cables and curtain wall components may be ignited. On the other hand, glass within PV panels will break and fall out when exposed to a fire [15–18], not only creating new fire spread pathways that facilitate vertical fire propagation but also allowing fresh air into the interior, which significantly accelerates the burning rate of flammable materials. Furthermore, falling combustible debris from PV panels may ignite lower or surrounding combustibles, thereby further promoting fire spread [19].

Most existing studies have primarily focused on small-scale PV panel combustion tests [20,21], emphasizing the performance of individual modules [22] or internal combustible materials [23–25]. However, such single-material or individual module tests may not reflect the fire behavior of BIPV façades under real conditions. In particular, the effects of large-scale façade geometry, combustion characteristics, and ventilation variations cannot be captured in small-scale experiments. At a larger scale, research has primarily focused on rooftop PV modules [26–28] or panels mounted as additional building elements, rather than vertical BIPV façades. In practical BIPV systems, PV modules are integrated as part of the building envelope rather than added as external attachments. When exposed to a fire, the combustion of encapsulation materials and the breakage and fallout of glass within PV panels could strongly interact with compartment fires, accelerating fire spread and posing severe fire hazards. Although countries such as the UK,

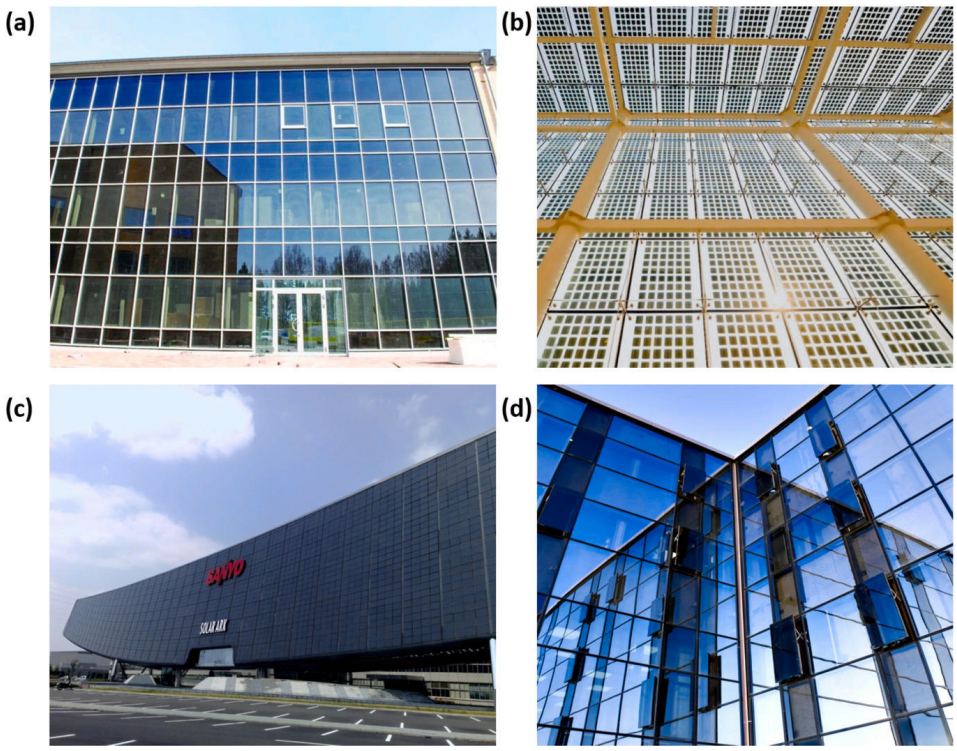

Fig. 1. Typical photovoltaic and glass façade. (a) CdTe façade [8]; (b) Double-glazed crystal silicon PV façade [9]; (c) Solar Ark in Japan (partly employing single-glass crystalline silicon PV panels) [10]; (d) Glass façade [11].

Switzerland, Canada, the USA, and Australia require large-scale façade tests for combustible exterior wall materials, little attention has been paid to the large-scale PV curtain walls (sometimes treated as non-combustible), and even corresponding façade tests are still lacking. Moreover, the diversity of PV module configurations (e.g., single-glass and double-glazed modules) further complicates fire behavior, yet reliable large-scale fire data for BIPV façade systems remain extremely limited. This gap hinders accurate fire risk assessment and the development of effective fire safety design strategies for façade systems.

In this work, a large-scale experimental setup was designed to study the thermal breakage and fallout of BIPV façade in an enclosure fire. Three representative types of photovoltaic curtain modules were selected for the experiments: cadmium telluride (CdTe) thin-film, double-glazed (DG), and single-glass (SG) crystalline silicon modules. Traditional glass was used for comparative experiments. Critical parameters were recorded, including the breakage time, PV panel and glass surface temperature, the radiant heat flux at the ambient side of the panel surface, mass loss rate of fuel, compartment temperature, heat release rate of fire, the total/radiant heat flux at the fireside of the compartment. To sum up, this study provides systematic large-scale experimental evidence on BIPV façade fire behavior, quantifies the critical breakage characteristics and temperature differences for different kinds of PV panels, and reveals the feedback effects of BIPV façade fallout on compartment fire dynamics, including flame ejection behavior, compartment temperature evolution, heat release rate development, and heat flux variations. The findings offer important implications for fire safety assessment and design of BIPV façades.

2. Material and methods

As shown in Fig. 2, an experimental compartment with dimensions of 1400 (length) × 1400 (height) × 1800 (width) mm^3 was built to resemble the fire conditions in BIPV façade. It was constructed from stainless steel and internally lined with 80 mm-thick ceramic fiber boards to reach insulation. A stainless-steel frame was installed on the open side of the compartment, with a small opening reserved at its center for mounting the heat flux gauge. Two PV panels, named Panels A (left) and B (right), each with a size of 600 mm × 600 mm, would be fixed on the frame by the clamps to form a PV façade. The frame covered the outer 30 mm edge of the test sample, creating a central heated area of 540 × 540 mm^2. In addition, 10-mm-thick ceramic fiber papers were covered with the edges of the sample and secured into the frame, which could reduce the influence of heat conduction and may as well prevent localized stresses of uneven pressure from the metal frame. Two openings (each with dimensions of 600 mm × 600 mm) were located at the lower part of the compartment to allow natural ventilation. Each set of experiments was conducted twice.

The measurement systems included the sheet and sheathed thermocouples (TCs), heat flux (HF) gauge, mass loss balance, digital camera and data acquisition. As illustrated in Fig. 2, there are 42 thermocouples in the compartment and 20 thermocouples on both sides of the PV panels. Seven thermocouple trees (named TCT 1–TCT 7), each equipped with six 1 mm diameter K-type thermocouples, were placed in the compartment to measure gas temperature, as shown in the overhead view of the compartment. In addition, sheet thermocouples were set at the four-sided shielding area and the geometric center of the front and back surfaces of the PV panel, to measure the surface temperature through high heat-conducting sheets, which were composed of a highly conductive aluminum alloy. With dimensions of 20 × 10 mm^2, the thermocouples increased contact areas between the temperature-sensing elements and the detected objects. The measurement of thermocouples ranges from 0 to 1200 °C, which is adequate for conducting these tests. For the

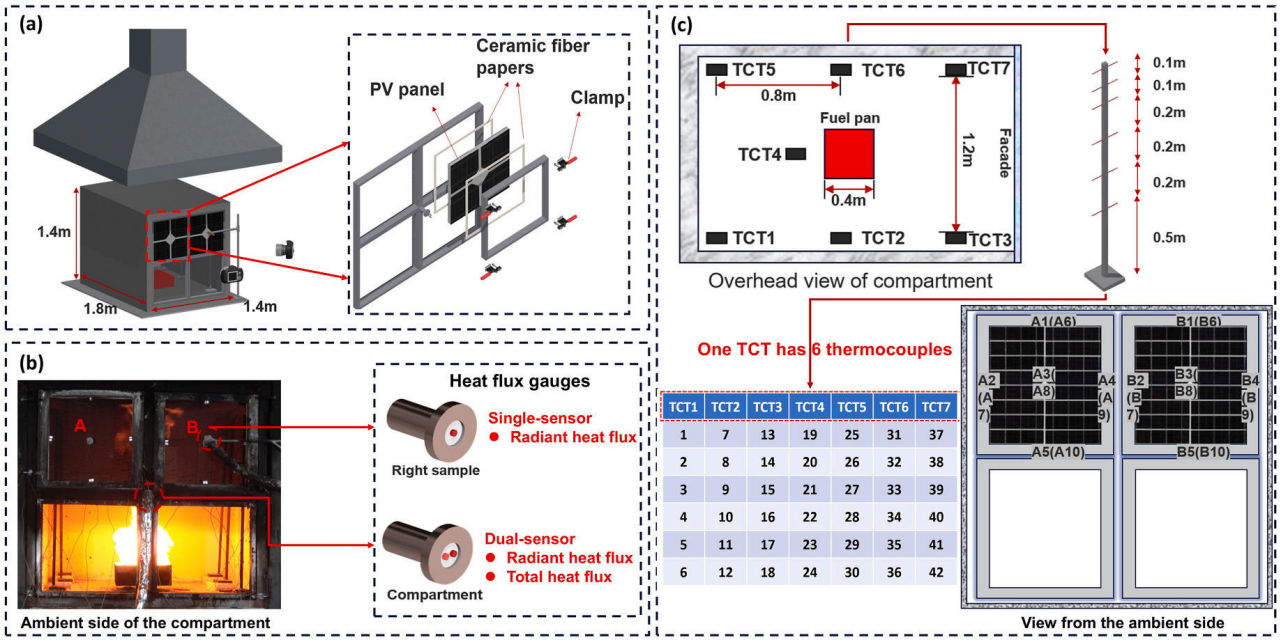

Fig. 2. (a) Experimental setup; (b) Layout of heat flux gauges; (c) Layout of thermocouples in the compartment and PV panels at fire-exposed and ambient sides.

purpose of analysis, bracketed numbers represent the thermocouples attached to the sides exposed to fire, whereas un-bracketed numbers indicate the thermocouples situated on the ambient sides. Two Schmidt–Boelter heat flux gauges were installed. A dual-sensor gauge was located at the center of the compartment frame to measure both the total and radiant heat flux of the compartment, whereas a single-sensor gauge was mounted on a bracket 55 mm away from the surface of the right sample to measure the radiant heat flux received by the façade. All the thermocouples and flux gauges were connected to a high-precision data acquisition instrument through armored cables, with a sampling frequency of 1 Hz. A fuel pan with dimensions of 400 mm (length) × 400 mm (width) × 150 mm (height) was placed in the center of the compartment floor. To ensure the repeatability of the fire source, 6 L of n-heptane were measured using two measuring jugs for each test. Above the burning compartment, a smoke-collecting hood with dimensions of 6000 mm × 6000 mm was located, and the heat release rate (*HRR*) could be calculated using the oxygen consumption method. Furthermore, two digital cameras were positioned at the front and side of the compartment to record the fire behavior and development.

All the above equipment was time-calibrated before the experiment to achieve synchronous measurements. The Schmidt–Boelter heat flux gauges were factory-calibrated, and the calibration certificates were verified before the experiments. The uncertainty of the heat flux measurements was estimated to be within ±3% (according to the manufacturer's manual). The thermocouples were also pre-calibrated by the manufacturer, and both thermocouples and heat flux gauges were functionally tested using an ignition torch, ensuring the accuracy and reliability of the measurement data prior to each experiment. It should be noted that in some cases, thermocouples detached due to the impact caused by flame or the breakage of samples. In these instances, both the videos and thermocouple plots were analyzed together to ensure that any anomalous data resulting from these impacts were excluded from the analysis.

The *HRR* and average compartment temperature in Tests 1 and 2 of Case 1 are shown in Fig. 3. The average temperatures are shown as solid lines, with the corresponding standard error shown as shaded areas. It can be seen from Fig. 3 that the *HRR* and temperature curves from the two repeats show consistent trends. Among all the repeated tests, the maximum repeatability error for the first breakage time was 15.2% (Case 4), and the maximum error in the peak HRR was 9.4% (Case 7), indicating good experimental repeatability.

The two main types of PV panel technology are thin-film and crystalline silicon. Thin-film PV panels are created using the deposition process where in the thin semiconductor layers are put onto a substrate material such as glass or metal, electrically linked and sealed to shield them from environmental elements [29]. This differs from wafer-based (e.g., Si) technologies wherein wafers are individually processed into cells, soldered together, and packaged into modules.

Three typical curtain wall components were tested in this study: CdTe, c-Si, and 3.2-mm glass. It should be noted that for the c-Si material, additional tests were conducted for both DG (double-glazed) and SG (single-glazed) configurations. As shown in Table 1, the experimental cases were conducted for: (1) double-glazed CdTe PV panel (DG CdTe) of TCO (a special transparent conductive oxide glass) and rear cover glass with solar cell and 1.52 mm interlayer of PVB film, (2) double-glazed crystalline silicon PV panel (DG c-Si) consisting of two glass panes with two 0.76 mm interlayer of PVB film and solar cell, (3) single-glass crystalline silicon PV panel (SG c-Si) with solar cell and two 0.5 mm interlayer of EVA and TPT (a multilayer product), and (4) single glazing (SG). The junction box and cable behind each PV panel were removed to eliminate the influence of its own combustion on the experimental results. Furthermore, the Control 1 in the diagrams means a fully open façade condition without PV panels, providing an initial ventilation opening without glazing or combustible materials. In Control 2, a non-combustible fireproof board was employed, which remained intact throughout the experiments and provided an intact, non-breakable façade boundary condition. These two control cases represent fully open and semi-open (no ventilation change) boundary conditions, respectively, and were suitable for comparison with the other experimental cases. Except for the control groups, each experimental case was repeated twice.

The glass used in PV panels can be divided into two types: annealed (non-tempered) and tempered glass. It is worth noting that due to the existing technology, TCO glass, which is on the outside of the building, can only be non-tempered glass, while rear cover glass

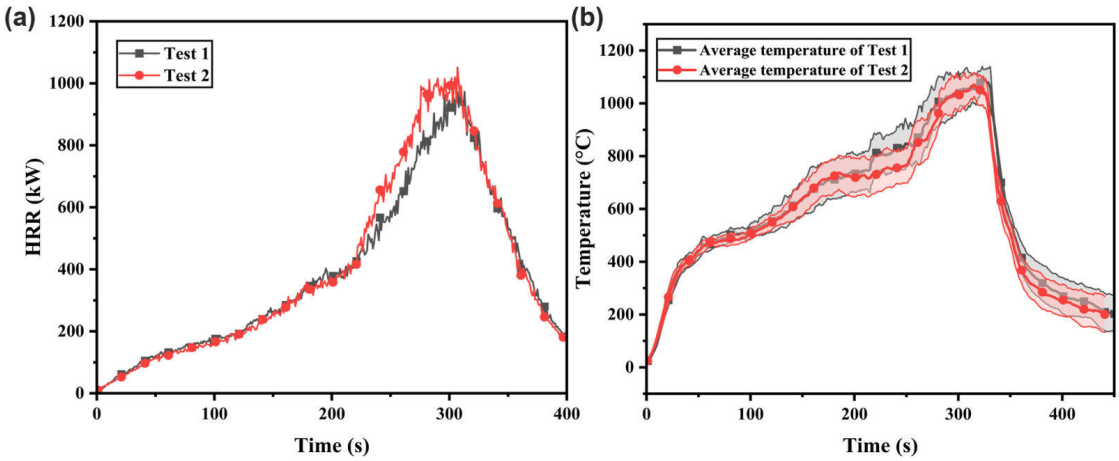

Fig. 3. (a) Heat release rate in Tests 1 and 2 (Case 1); (b) Average compartment temperature (10 cm from the ceiling) in Tests 1 and 2 (Case 1).

Table 1
Experimental case and construction of different kinds of PV panels and glass.

Cases	Test number	Construction of PV panel (from outside to inside the enclosure)
Case 1- DG CdTe (A)	Test 1 Test 2	3.2 mm TCO glass (A) + solar cell + 1.52 mm PVB+ 3.2 mm glass (A)
Case 2- DG CdTe (T)	Test 1 Test 2	3.2 mm TCO glass (A) + solar cell + 1.52 mm PVB + 3.2 mm glass (T)
Case 3-DG c-Si (A)	Test 1 Test 2	3.2 mm glass (A) + 0.76 mm PVB + solar cell + 0.76 mm PVB + 3.2 mm glass (A)
Case 4-DG c-Si (T)	Test 1 Test 2	3.2 mm glass (T) + 0.76 mm PVB + solar cell + 0.76 mm PVB + 3.2 mm glass (T)
Case 5- SG c-Si (A)	Test 1 Test 2	3.2 mm glass (A) + 0.5 mm EVA + solar cell + 0.5 mm EVA + 0.3 mm TPT
Case 6- SG c-Si (T)	Test 1 Test 2	3.2 mm glass (T) + 0.5 mm EVA + solar cell + 0.5 mm EVA + 0.3 mm TPT
Case 7- SG (A)	Test 1 Test 2	3.2 mm glass (A)
Case 8- SG (T)	Test 1 Test 2	3.2 mm glass (T)
Control 1	/	No panel and fireproof board
Control 2	/	Fireproof board

*Note: A denotes annealed glass, and T denotes tempered glass.

can be tempered or non-tempered glass. Correspondingly, the two glass panes within the crystalline silicon PV panel are uniformly tempered glass or non-tempered glass. The cross-sections of the four different types of glazing are sketched in Fig. 4. All the glass panes were installed in the form of exposed framing glazing, and the condition of an actual glazing unit was approximated as closely as possible.

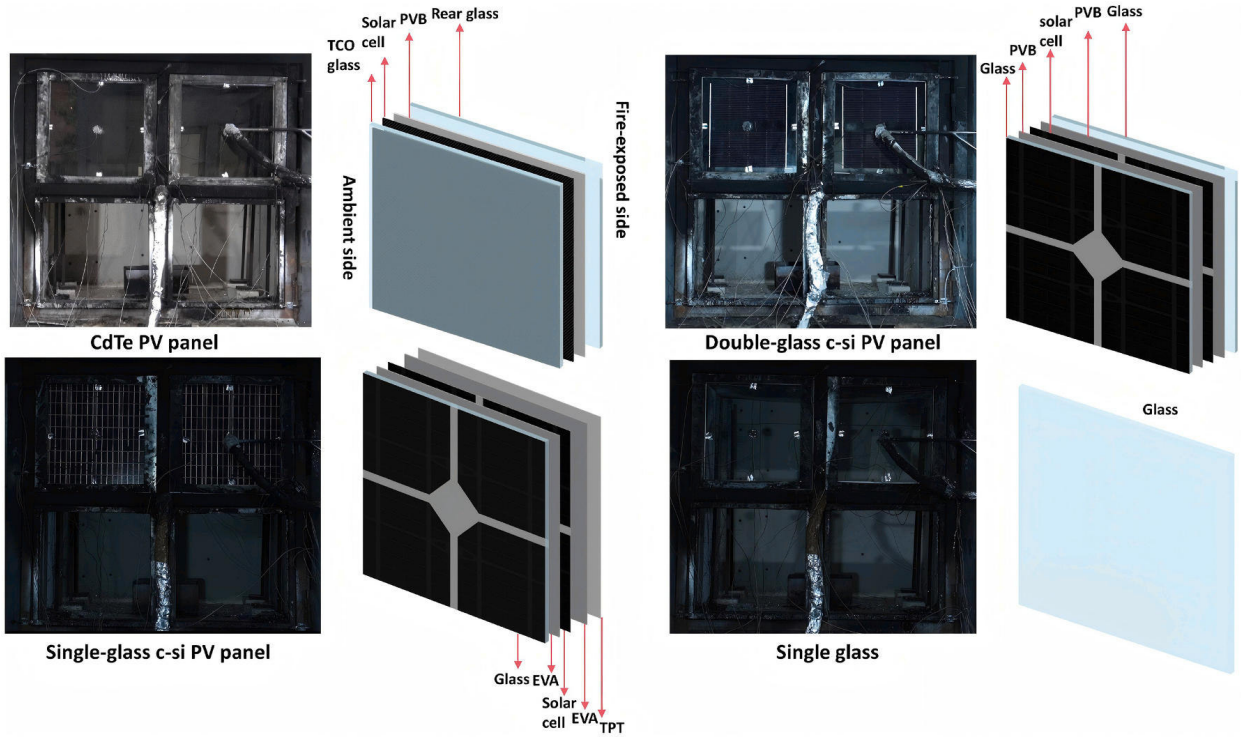

Fig. 4. Experimental scene before ignition and the structure of tested samples.

3. Results and discussion

3.1. Breakage time and fracture behavior

Fig. 5 shows the experimental phenomena for different cases. The time to first breakage, as well as the moments when panels A and B fell out to form openings, are listed. In some cases, the specimens did not fall out to form openings; therefore, some images are blank (e.g., in Test 2 (Case 4), only the inner pane of panel B detached). It should be noted that the time (t = 0 s) was defined as the moment of fuel ignition, and the ignition-stage photographs were taken at t = 10 s to avoid camera obstruction during manual ignition. Additionally, the extinction time refers to the moment when the flame disappears. For BIPV façade fires, the fire performance is significantly more complex than that of traditional glass façade fires, as it involves not only the melting and combustion of internal combustible materials but also the breakage and fallout of glass. In the above six PV panel cases, almost all panels broke, and burning laminated layers and glass debris fell to the ground below the façade and continued burning throughout the test (as seen in Fig. 6(a)). The risk of falling panels and debris is not acceptable as they can easily ignite combustibles inside the building façade, posing a greater risk of fire. Furthermore, the falling parts could also pose a significant safety risk to occupants during egress by obstructing evacuation paths, causing injuries, or creating conditions that hinder timely and safe evacuation. Even after the heptane fire had burnt out, the combustible layers in the PV panels continued to burn, as shown in the final images of each PV panel case. In addition, there were significant differences in the cracking and fallout behavior of PV panels with annealed glass or tempered glass structures, as well as differences in the order of melting of internal combustible materials.

Taking the typical Case 1 as an example, the breakage of the inner glass was first observed, followed by the melting, flowing, and emitting gases of the PVB interlayer. As cracks continuously propagated and eventually intersected to form glass islands, as well as the adhesive effect of the interlayer PVB failed, portions of the inner glass fell out, as shown in Fig. 6(b). It is noteworthy that the location of crack initiation in the outside glass was nearly the same as the inner glass due to the close bonding. Furthermore, it was observed that the interlayer began to sustain burning and some of them along with PV panel fragments started dripping onto the ground during the test. In the later stage of the experiment, the right broken outer glass and most of the bonded inner glass within the PV panels fell out as a whole, forming new ventilation openings. However, the left PV module did not immediately fall out as a whole but instead

Fig. 5. Fire behavior of double-glazed PV modules. (a) Test 2 (Case 1); (b) Test 2 (Case 2); (c) Test 2 (Case 3); (d) Test 2 (Case 4).

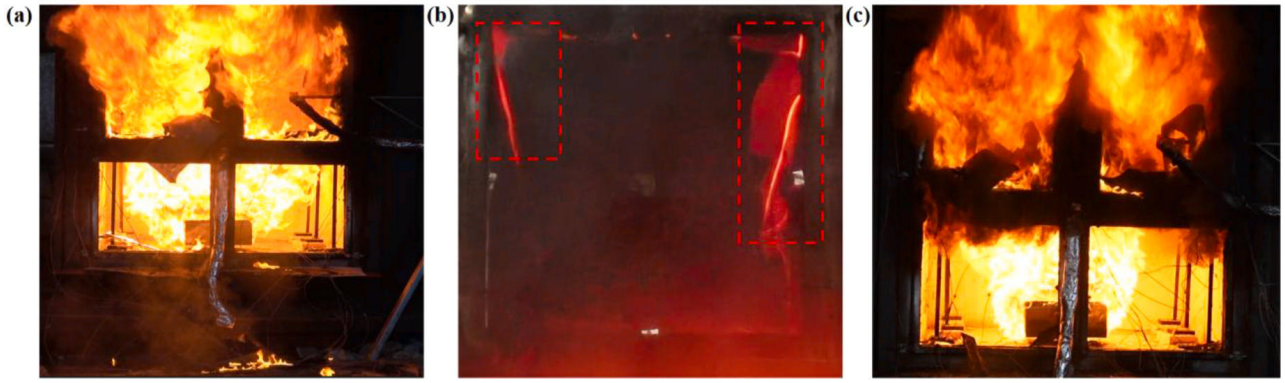

Fig. 6. Experimental phenomena. (a) Burning debris falling to the ground; (b) Fallout of inner glass within the left CdTe PV panel A (Test 2 of Case 1); (c) Softened PV panels (Test 2 of Case 3).

showed a softened and deformed state. This phenomenon can be attributed to the combined effects of interlayer adhesion and the fracture characteristics of annealed glass, where the fractured fragments were restrained and suspended on the module surface by the PVB interlayer due to its incomplete thermal decomposition. As the flame ejection intensified, the broken fragments eventually fell out. The same phenomenon was also observed in Case 3, where more PV modules were in a softened and deformed state (probably due to the effect of the double PVB interlayers), as shown in Fig. 6(c). In addition, the fallen parts of double-glazed crystalline silicon PV panels contained not only panel fragments but also solar cells, which results from the fact that the thin-film PV panels are coated on glass panels, while the solar cells in crystalline silicon PV panels are contained in PVB interlayers.

Although the number of initial glass panes was the same in Case 2, the change of the rear cover glass to tempered glass resulted in

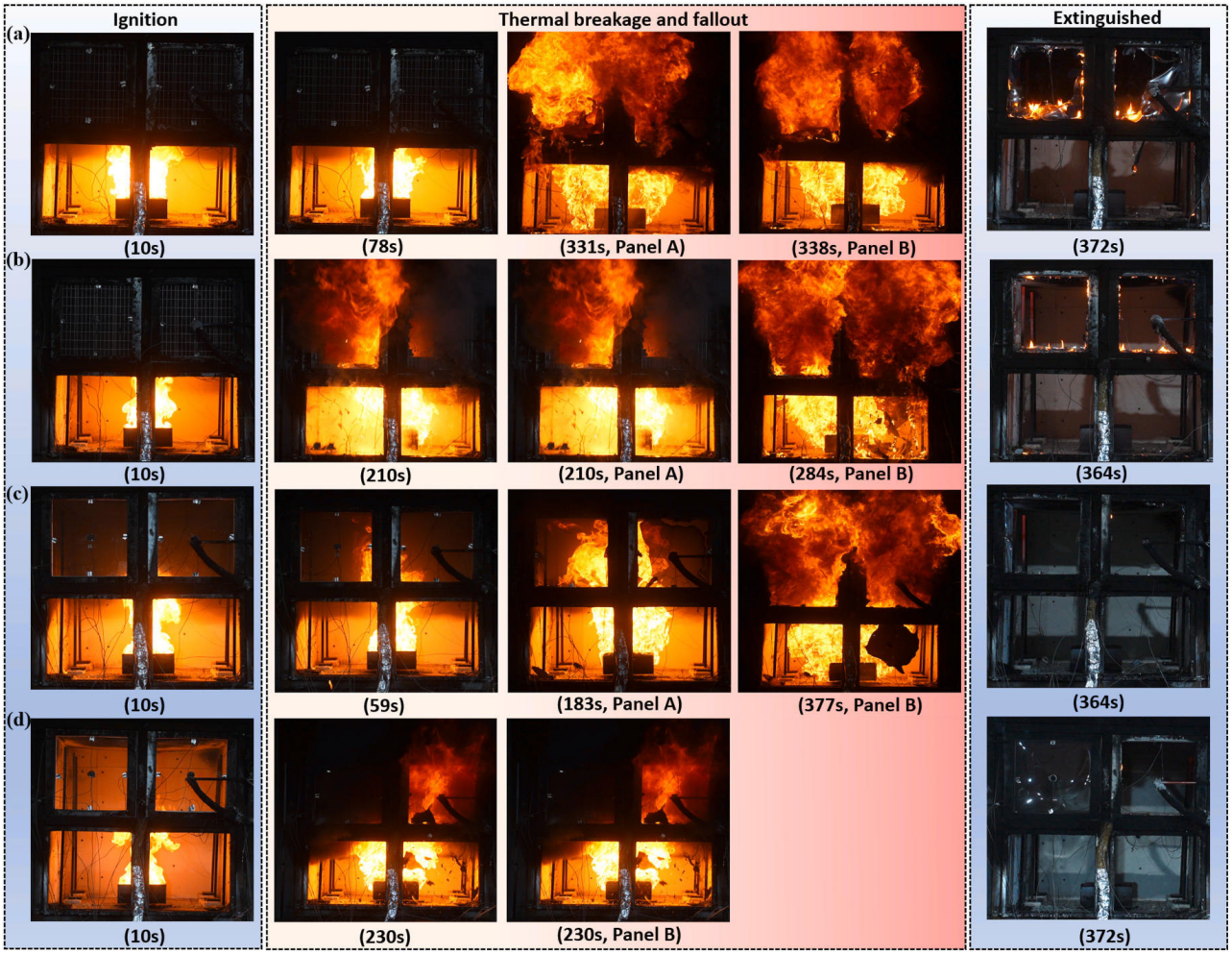

Fig. 7. Fire behavior of single-glass PV modules. (a) Test 1 (Case 5); (b) Test 2 (Case 6); (c) Test 1 (Case 7); (d) Test 1 (Case 8).

markedly different fire behavior compared with Case 1. Owing to the much higher strength of the internal tempered glass compared with annealed glass, the fracture of the outer TCO glass (annealed glass) and the melting of the internal combustible layer were first observed. Subsequently, with further temperature accumulation, the internal tempered glass eventually broke, and the entire PV panel fell out. The failure process was also different in Case 4. The melting of the internal PVB was first observed, followed by the breakage and fallout of the inner tempered glass, which completed within 1s. Despite the detachment of the inner glass, the outer glass panel could still function as a barrier, preventing the formation of a new vent until the outer glass fell out.

Compared with double-glazed PV modules, single-glass PV modules are encapsulated by the combustible TPT backsheet. Unlike double-glazed modules, where the rear cover glass effectively attenuates heat transfer, single-glass modules expose the combustible backsheet directly to the flame, resulting in accelerated pyrolysis of the material. In the case of single-layer annealed glass PV panels, the observations were consistent with previous bench-scale experiments [30]. It was observed that the glass fractured and the pyrolysis of EVA film and TPT backsheet occurred. As the test continued, cracks continuously propagated and eventually intersected, leading to island. However, unlike the single-layer annealed glass in Case 7, even after crack islands had formed, the single-glass crystalline silicon PV panel did not fall out immediately after breakage. This difference was primarily attributed to the composite structural characteristics of the PV module. The front glass layer was firmly bonded with the EVA interlayer and TPT backsheet through the lamination process. When the glass fractured under elevated temperatures, the broken fragments were not instantaneously unsupported but were retained by the adhesion of the EVA and the confinement imposed by the backsheet, thereby remaining attached to the panel surface. Meanwhile, the EVA was gradually softened and partially combusted under fire conditions, exerting a tensile effect on the glass fragments, which caused them to assume a suspended or stretched state, resembling a softening phenomenon, as shown in Fig. 7(a). Eventually, as the fire intensified, the fragments progressively fell out, which ultimately resulted in the formation of new openings. While in the case of single-layer tempered glass PV panels, melting and dripping of the backsheet material were first observed, followed by the fallout of the tempered glass. Unlike single-layer annealed glass PV panels, the pre-stress of tempered glass caused overall breakage immediately. It is noteworthy that in Case 7 with single-layer annealed glass (Fig. 7(c)), the initial fracture was accompanied by the fallout of a small portion of glass fragments, which was attributed to the absence of adhesive interlayer restraint. In contrast, the fracture and fallout characteristics in Case 8 were observed to be consistent with those of single-layer tempered PV panels.

The first time to breakage and large-area opening of PV panel and single glazing are listed in Table 2. In the present experiments, the time at which the majority of PV panels fell out to create an opening was defined as the large-area opening time (nearly fully open, with a small amount of debris remaining), with the final state referring to the condition when the flame was extinguished. For single-glass PV panels, the opening was formed once the glass fell out. In contrast, for double-glazed PV panels, such an opening was established only after both the inner and outer glass layers fell out. By comparison, the maximum repeatability error of the time to first breakage, defined as the maximum relative deviation between repeated tests, was 15.2% (Case 4), indicating good experimental repeatability. Among all experimental cases, PV panels made of annealed glass and single-layer tempered glass PV panels broke and fell out (Cases 1–6), while double-layer tempered glass PV panels partially fell out. It is noteworthy that in Case 8 with single glazing, only one single-layer tempered glass pane broke and fell out in each of the two repeated tests. This difference could be attributed to the presence of combustible materials in PV panels, such as EVA, PVB films, and TPT backsheet. These additional fire loads melt under high temperatures, undermining the structural integrity of the panels and thereby exacerbating fire risks.

The experimental results indicate that the type of glass is a key factor in determining the thermal breakage and fallout performance

Table 2
First failure and large-area opening time of the tested PV panels and glass.

Cases	Test number	First break time (s)	Average (s)	First Large-area opening time (s)	Average (s)	Final state
Case 1-CdTe (A)	Test 1	78	74	212	230	A_{in}, A_{out}, B_{in}, B_{out}
	Test 2	70		248		A_{in}, A_{out}, B_{in}, B_{out}
Case 2-CdTe (T)	Test 1	146	146	228	224	A_{in}, A_{out}, B_{in}, B_{out}
	Test 2	145		220		A_{in}, A_{out}, B_{out}
Case 3-DG c-Si (A)	Test 1	66	67	304	295	A_{in}, A_{out}, B_{in}, B_{out}
	Test 2	68		286		A_{in}, A_{out}, B_{in}, B_{out}
Case 4-DG c-Si (T)	Test 1	173	189	301	283	A_{in}, B_{in}, B_{out}
	Test 2	204		264		A_{in}, A_{out}, B_{in}
Case 5- SG c-Si (A)	Test 1	78	80	331	333	A, B
	Test 2	82		334		A, B
Case 6- SG c-Si (T)	Test 1	224	217	224	217	A, B
	Test 2	210		210		A, B
Case 7- SG (A)	Test 1	59	54	183	177	A, B
	Test 2	49		170		A, B
Case 8- SG (T)	Test 1	230	223	230	223	B
	Test 2	216		216		B

*Note: A and B denote the left and right samples (from the ambient side view of the compartment), respectively. In denotes inner glass (fire-exposed side), and out denotes outer glass (ambient side).

of PV modules. For PV modules made of annealed glass (Cases 1, 3, 5, and 7), the initial breakage generally occurred within 67–80 s, whereas for those made with tempered glass (Cases 4, 6, and 8), the first breakage time was significantly extended to 189–223 s, increasing approximately 2–3 times. Even in Case 2, the outer TCO glass within CdTe modules first broke, resulting in the longest first breakage time among all annealed PV panel cases. This improvement is primarily attributed to the surface compressive stress layer formed during the secondary heat treatment process of tempered glass, which effectively suppresses crack initiation and propagation, thereby delaying thermal failure.

In addition, the influence of the double-glazed PV panels on the first breakage time was found to be limited when compared with the single-glass structure. Actually, the double-glazed crystalline silicon PV panels in Case 1 and Case 3 failed earlier than the single-glass PV panels in Case 5, with the same trend observed in Case 4 (189 s) and Case 6 (217 s). However, the double-glazed PV modules effectively suppressed the formation of new ventilation openings after breakage, especially in the case of tempered glass, as a vent was formed only after the outer glass had fallen out. This effect was observed in Cases 4 and 6, where the occurrence of large-area openings was delayed by approximately 66 s. It is noteworthy that in single-layer annealed-glass PV modules, the time to the first large-area opening was longer than that for tempered-glass PV modules under the same conditions. This delay was caused by the adhesive effect of the internal combustible materials and the characteristics of annealed glass, which prevented the glass from falling immediately after breakage and resulted in gradual softening and detachment3.1.

In terms of the influence of backsheet materials, single-glass crystalline silicon PV panels were constructed with combustible TPT backsheet, whereas most other samples featured non-combustible glass. The single-glass crystalline silicon panels (Case 5, 80 s) showed a longer time than single-glass panels (Case 7: 54 s) under the same annealed glass conditions, as well as the time to large-area openings. This difference was primarily attributed to the composite structural characteristics of the PV module. What is more, burning parts and debris produced by the backsheet should not be overlooked, as they can lead to flame spread and heightened fire risk.

3.2. Breakage time and temperature difference

As previously studied, the local high stress caused by the temperature difference is the main cause of glass breakage within PV panels [31]. To investigate this issue, the temperature difference on the PV panel surface is defined as:

$$\Delta T_{in} = A_8 - \frac{A_6 + A_7 + A_9 + A_{10}}{4} or B_8 - \frac{B_6 + B_7 + B_9 + B_{10}}{4}$$
$$\Delta T_{out} = A_3 - \frac{A_1 + A_2 + A_4 + A_5}{4} or B_3 - \frac{B_1 + B_2 + B_4 + B_5}{4} \quad (1)$$

The temperature differences between the fireside and backside of the inner and outer glass layers at the moment of breakage for different cases are listed in Table 3. It should be noted that some thermocouples detached due to the impacts induced by glass breakage or flame impingement, leading to missing temperature records at the breakage moment. These cases are marked as "/" in Table 3. Although variations in breakage time were different under different conditions, a clear trend can be observed. For annealed-glass PV panels, whether single-layer or double-layer structures, the average temperature difference ranged from 35 to 59 °C, whereas for tempered-glass structures, the corresponding values were significantly higher, ranging from 207 to 273 °C. It should be mentioned that for the outer glass in the double-glazed PV panels, thermocouples were positioned on the outer surface, leading to measured temperature differences lower than the actual values (with Case 2 as an exception, where the outer TCO glass first fractured). Furthermore,

Table 3
Temperature difference of the inner and outer of the PV panel and glass at the moment of breakage.

Cases	Test number	Inner-breakage temperature difference (°C)	Average (°C)	Outer-breakage temperature difference (°C)	Average (°C)
Case 1-CdTe (A)	Test 1	52	50	38	38
	Test 2	48		38	
Case 2-CdTe (T)	Test 1	66	59	/	273
	Test 2	52		273	
Case 3-DG c-Si (A)	Test 1	55	54	31	35
	Test 2	53		38	
Case 4-DG c-Si (T)	Test 1	255	226	/	207
	Test 2	197		207	
Case 5- SG c-Si (A)	Test 1	45	50	none	none
	Test 2	55		none	none
Case 6- SG c-Si (T)	Test 1	264	226	none	none
	Test 2	187		none	none
Case 7- SG (A)	Test 1	36	34	none	none
	Test 2	31		none	none
Case 8- SG (T)	Test 1	187	187	none	none
	Test 2	/		none	none

in Cases 5 and 6, measurement points located on the backsheet would also introduce additional errors. Single-layer glass was also tested under the same conditions for comparison, and it showed a slightly lower average breakage temperature difference compared with single-glass PV panels, which could be attributed to the absence of constraint provided by the laminated layers.

3.3. Impact of façade fallout on the compartment fire

Two methods were used to measure the heat release rate in these experiments. One involved measuring the mass loss of the fuel pan via a high-precision balance and calculating the heat release rate based on the combustion efficiency. In addition, a large-scale smoke-collecting hood was set above the compartment to collect the gas and smoke, and the heat release rate was calculated on the basis of the oxygen consumption method. As shown in Fig. 8, two typical cases were selected for comparison to demonstrate the feedback effect of façade fallout on the fire development process and the heat release rate, and the red dashed lines in the *HRR* plots denote the time at which the panel fallout occurred. The results show that the *HRR* measured by both the smoke hood and the balance exhibited almost the same temporal trend, which can be divided into three stages: rapid growth followed by stable combustion and eventual decay. The *HRR* reached its maximum value during the stable combustion period. However, significant differences in the fire developing process were observed due to the structural variations of the PV panels.

In the Test 1 of Case 2, the early-stage combustion mainly occurred within the compartment, with the *HRR* increasing slowly and smoke spilling out through the bottom openings. As the fire intensified, the left PV panel A fell out at 228 s, altering the stable ventilation condition and creating a new opening that induced flame ejection, leading to an accelerated *HRR* growth. Subsequently, at approximately 266 s, the right PV panel B fell out, resulting in dual flame ejections through the window. The enhanced interaction between the compartment and the exterior caused the fire to develop rapidly and reach its peak. Afterwards, the *HRR* became relatively stable during the platform period. Finally, with the depletion of the heptane and the inflow of fresh air accompanied with the fallout generated the cooling effect, the *HRR* gradually declined and entered the decay phase. In contrast, in the Test 1 of Case 4, the PV panels showed higher structural integrity and remained intact even after the occurrence of flashover. Consequently, flames first spilled out through the bottom opening and spread upward quickly. The intensity of flame ejections from the bottom opening is significantly higher than that in Case 1. With further heat accumulation, panel B fell out at 301 s, producing an intense flame ejection from the window, while the intact panel A continued to be heated by the bottom flame spillover until the end of the test. To sum up, the strength and type of PV panels not only affect the development of compartment fires but also directly determine the pattern and intensity of flame ejection, thereby exerting a significant influence on the risk of photovoltaic façade fire spread.

To investigate the characteristics of the compartment temperature, the measuring points of the smoke layer 10 cm away from the ceiling (TC1, TC7, TC13, TC19, TC25, TC31 and TC37) were selected for analysis. These thermocouples correspond to the top thermocouples of thermocouple trees TCT 1–TCT 7, respectively, and were used as representative points to characterize the ceiling-layer thermal field at different horizontal locations within the compartment (as shown in Fig. 9(e) and (f)). The dashed lines in Fig. 9 represent the time of the large-area opening generated due to PV panel fallout. It is noteworthy that in Case 4, complete fallout occurred in panel A, while only one of the glass layers in panel B fell out, leading to the formation of a single ventilation opening rather than a fully developed opening.

It can be seen from Fig. 9 that the temperature development can be divided into two stages: stage 1 (before the first large-area opening) and stage 2 (after the opening). In Stage 1, the growth rate of temperature changes from fast to slow. In Cases 3 and 4, as shown in Fig. 9(c) and (d), the temperature reached a long-period platform before the first large-area opening occurred. In addition, the time of the first large-area opening plays a crucial role in the compartment fire behavior. In Cases 1 and 2 (Fig. 9(a) and 9(b)), the

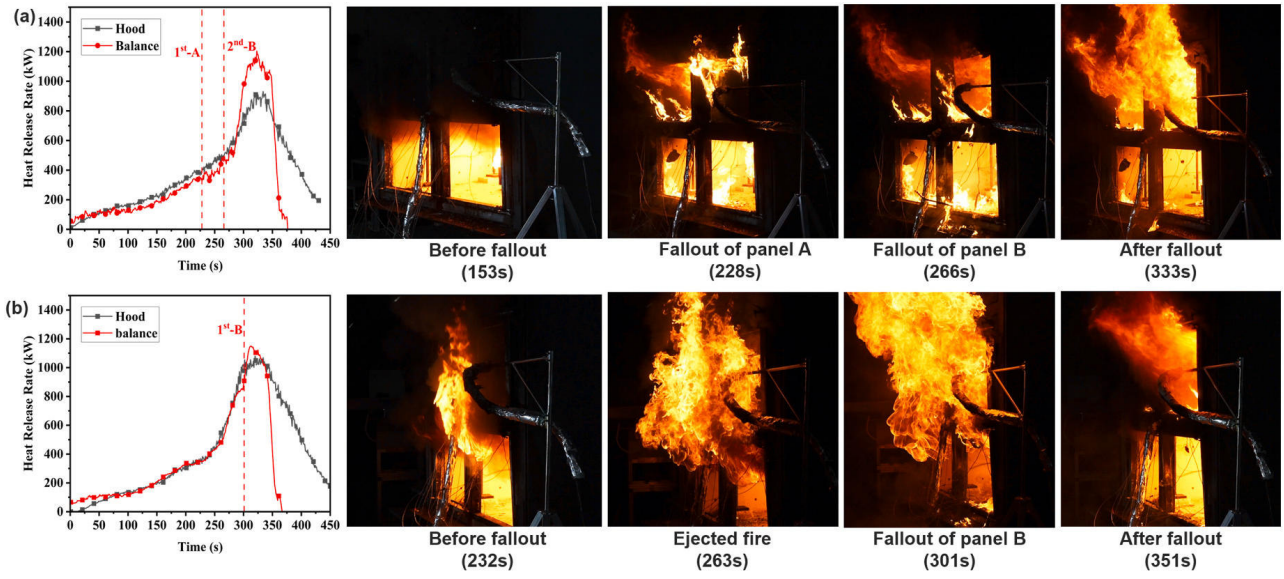

Fig. 8. Heat release rate changes in different cases. (a) Test 1 (Case 2); (b) Test 1 (Case 4).

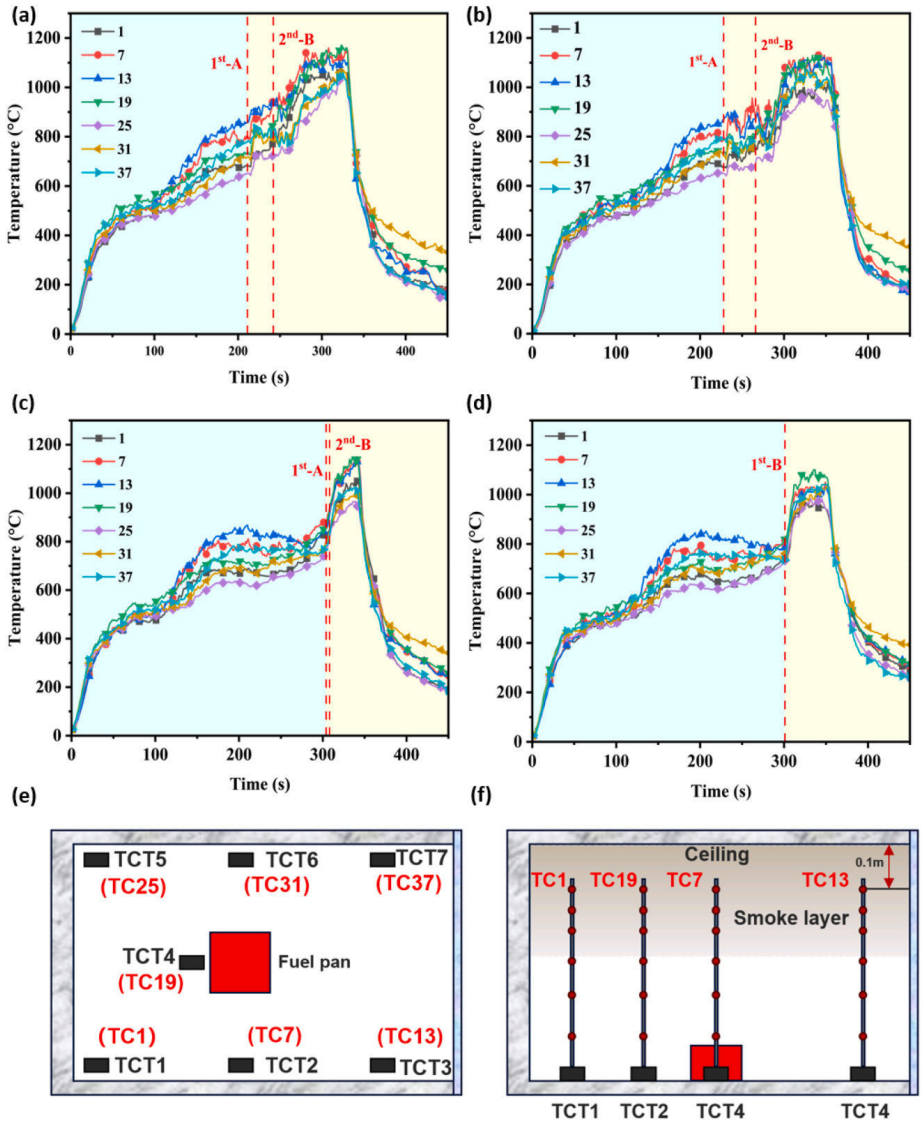

Fig. 9. Changes of the compartment temperature (10 cm from the ceiling) in different cases. (a) Test 1 (Case 1); (b) Test 1 (Case 2); (c) Test 1 (Case 3); (d) Test 1 (Case 4); (e) Overhead view of compartment; (f) Left view of compartment.

earlier façade fallout directly accelerated fire development. In contrast, delayed fallout in Cases 3 and 4 prolonged Stage 1, followed by a more rapid temperature rise in Stage 2. As the temperature continued to increase, the PV panel façade began to fall out, with the temperature entering Stage 2. The sudden change of the boundary conditions caused a large amount of fresh air to flow into the enclosure. As a result, the combustion reaction accelerated, and the smoke temperature increased rapidly.

The average temperatures at the measurement points (10 cm from the ceiling) for Case 2 (Test 1), Case 4 (Test 1), Case 6 (Test 2), Case 8 (Test 2), and Control 1 (fully open) and Control 2 (semi-open, no ventilation change) are shown in Fig. 10, with the standard errors presented as error bars. The two-stage trend was not observed under the conditions of Control 1 and Control 2. Under the fully open condition, a noticeable delay was observed in both the compartment temperature rise rate and the occurrence of flashover relative to cases equipped with PV panels. This was mainly due to the limited formation of an upper smoke layer, which reduced radiative heat feedback and consequently slowed the burning of fuel. Meanwhile, greater heat losses further suppressed fire growth. In contrast, in cases involving façade fallout, the compartment experienced rapid thermal escalation, as the newly formed openings allowed a large amount of fresh air to enter the enclosure. As a result, the average temperatures were notably higher than those in the control tests. In particular, in Case 2, the highest temperature reached nearly 1100 °C, which represented a 32.6% increase compared to the average temperature in Control 2, where the temperature remained below 820 °C.

In order to assess the impact of façade fallout on the spatial temperature distribution within the compartment, a non-dimensionalization approach was adopted. The critical time interval of 10 s before and after the first fallout event was selected, and seven representative measurement points were nondimensionalized.

$$TC_i^*(t) = TC_i(t) \Big/ (TC_1(t) + TC_7(t) + TC_{13}(t) + TC_{19}(t) + TC_{25}(t) + TC_{31}(t) + TC_{37}(t))_{average} \quad (2)$$

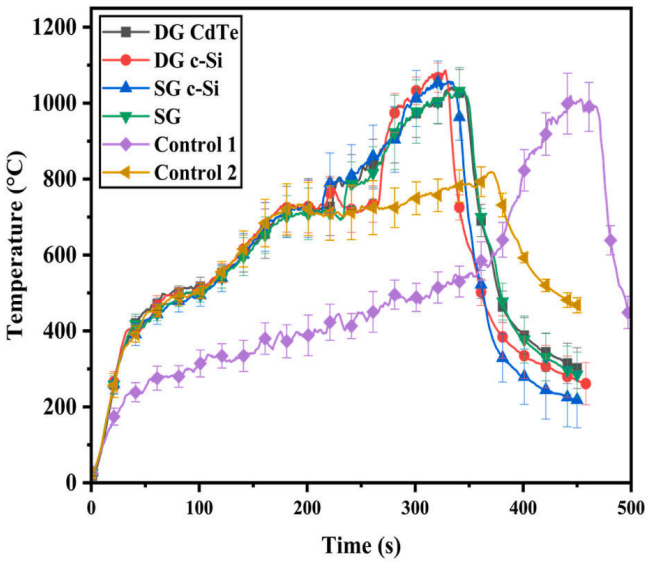

Fig. 10. The average temperatures (10 cm from the ceiling) in different cases.

where i denotes the measurement point, and t represents time.

The dimensionless temperature during the first fallout is shown in Fig. 11. Taking Test 1 (Case 4) as an example, the dimensionless temperature at all regions remained relatively stable before the first fallout. Specifically, the dimensionless temperature located at the rear of the compartment, far from the fire source (e.g., TC_1^*, TC_{25}^*), was significantly lower than 1, indicating that these regions have relatively low heat distribution. After the right-side sample B fell out, a strong positive response was observed at the measurement point TC_{37}^* (near the opening), where its value increased 9.4% compared to the moment of fallout. In contrast, the measurement point TC_{13}^*, which was located with respect to TC_{37}^*, showed an entirely opposite trend: it remained around 0.97 before the fallout of sample B, then rapidly dropped after the fallout, even reaching 0.92. This indicated that the fallout of sample B caused a sudden change in the compartment pressure, and the flame quickly deflected toward the newly created opening, causing this region to experience a brief thermal shock. As fresh air continued to enter through the opening, the cooling effect intensified, leading to the dimensionless temperature fluctuations. The spatial temperature distribution changed significantly within just a few seconds after the fallout, highlighting the strong impact of façade fallout on compartment thermal conditions and fire dynamics.

Fig. 12 shows the time-varying heat flux on the fire-exposed area of the façade in different cases. In these experiments, the total/radiant heat flux at the fireside of the compartment, as well as the radiant heat flux at the ambient side of the panel surface, was measured. In all experimental cases, the total heat flux gradually increased with fire growth, but significant fluctuations and subsequent rises were observed once PV panel fallout occurred, indicating that the newly formed opening strongly promoted fire development. The measured heat flux on the panel surface originated from two sources. One is the radiation transmitted through the right-side PV panel before its fallout, which is related to the transmittance of the tested sample. It is noteworthy that in crystalline silicon PV panels (Fig. 12(c) and (d)), the measured heat flux was relatively low due to the shielding effect of the solar cells. A similar phenomenon was also observed in Control 2 (Fig. 12(f)). The other source is the upward entrainment of flame spillover through the lower

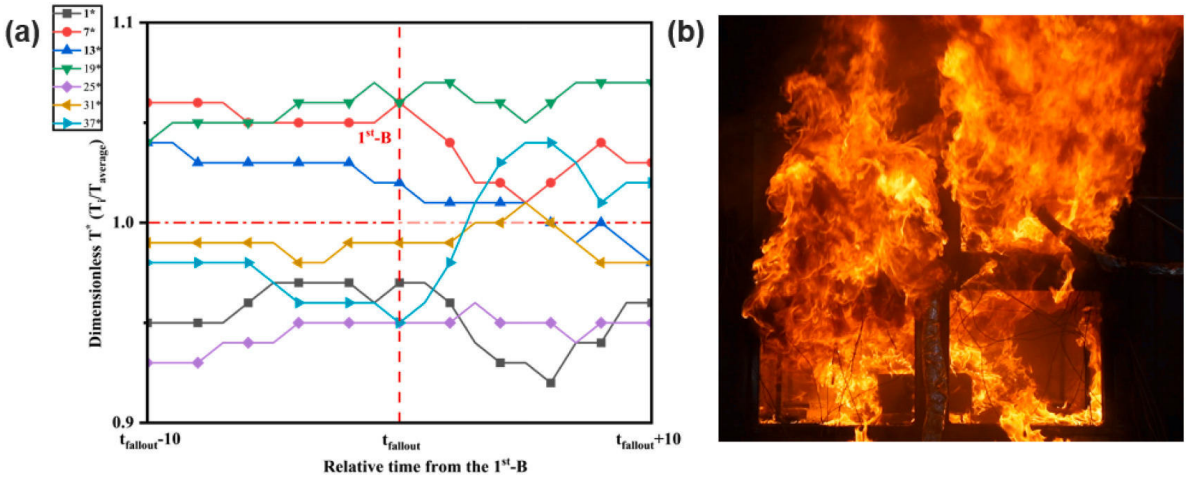

Fig. 11. Dimensionless temperature during the first fallout. (a) Test 1 (Case 4); (b) The Moment of fallout of Case 4.

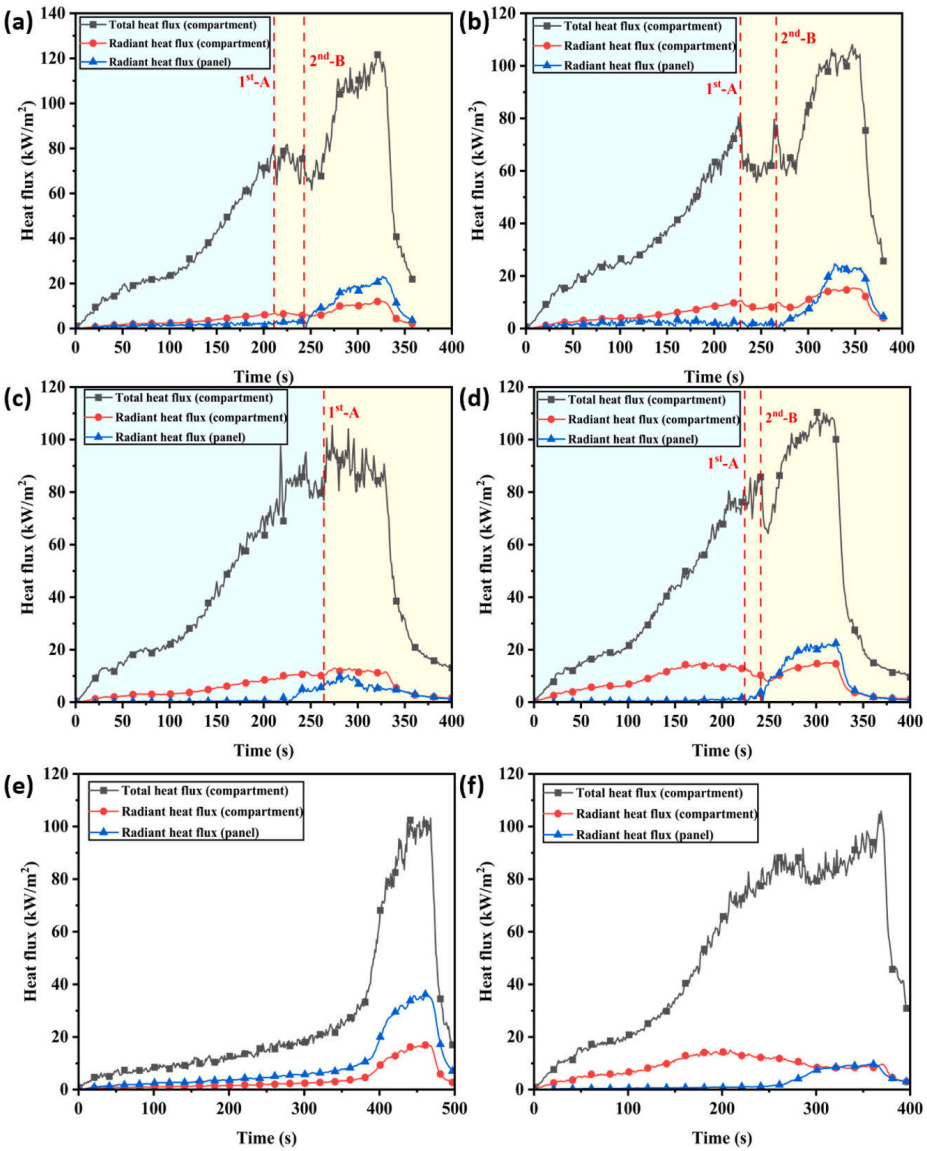

Fig. 12. The measured heat fluxes of the compartment and the panel. (a) Test 1 (Case 1); (b) Test 1 (Case 2); (c) Test 2 (Case 4); (d) Test 1 (Case 6); (e) Control 1; (f) Control 2.

opening. In Case 4 shown in Fig. 12(c), the right PV panel remained intact, and the measured heat flux increased with the intensification of the bottom flame ejection. In contrast, in other experimental cases, once the right PV panel broke, the heat flux rose rapidly and became the dominant contribution.

As shown in Fig. 12, the maximum total heat flux among all cases was 120 kW/m^2, and the critical total heat flux for PV panel fallout ranged from 70 kW/m^2 to 90 kW/m^2. Compared with the total heat flux, the contribution of radiative heat flux is relatively small, accounting for only about 8%. Therefore, the radiation plays a limited role in the breakage and fallout of PV panels in a compartment fire. Further comparison with the control groups reveals that in Control 1 (without PV panels), the façade opening remained fully open and the total heat flux increased relatively smoothly, whereas in Control 2 (with the fire-resistant board), the façade was partially ventilated and the maximum total heat flux was limited to about 106 kW/m^2. To sum up, the fallout of PV façade not only determined the timing of new opening but also triggered secondary fire intensification, resulting in total heat flux exceeding that observed under both fully open and semi-open (no ventilation change) conditions.

4. Conclusions

In this work, three representative types of curtain wall, including thin-film, double-glazed, and single-glass crystalline silicon, as well as traditional glass were selected for comparative experiments. It was established that there were significant differences in fire behavior between PV curtain walls and traditional glass curtain walls, and the types of glass within PV panels could significantly affect breakage and fallout behavior. In addition, the fallout of PV façade plays an important role in the development of compartment fires. The primary conclusions are as follows.

1) For BIPV façade fire, the fire performance is much more complex than traditional glass façade fire, as it involves not only the melting and ignition of internal combustible materials, but also the breakage and fallout of glass within PV panels. Moreover, self-sustained burning of interlayers was observed even after the fuel had burnt out, which could easily ignite combustibles inside the building façade, posing a greater risk of fire. In addition, due to the adhesive effect of the internal encapsulation materials and the characteristics of annealed glass, such PV panels entered a softened and deformed state after breakage as the temperature increased, and eventually fell out with the intensification of window flame ejection. While in tempered glass PV panels, owing to the pre-stress of tempered glass, the PV panel quickly fell out.
2) The type of glass is a key factor in determining the thermal breakage and fallout performance of PV modules. The first breakage time of PV modules with tempered glass was found to be significantly higher than that of those with annealed glass. Compared with the single-glass structure, the double-glazed PV modules effectively suppressed the formation of new ventilation openings after breakage. In addition, it was observed that the combustible interlayers inside the single-layer annealed-glass PV modules had an essential influence on the timing of the large-area opening, with the time longer than that of tempered modules under the same conditions.
3) Temperature gradients in glazing are the predominant cause of PV panel failure occurrence. Although failure times differed significantly between the cases, the critical temperature differences for the same type of glass within PV panels were relatively close. For annealed-glass PV panels, whether single-layer or double-layer structures, the average temperature difference ranged from 35 to 59 °C, whereas for tempered-glass structures, the corresponding values were significantly higher, ranging from 207 to 273 °C.
4) The strength and type of PV panels also influence compartment fire dynamics, governing both fire development and flame ejection behavior. Annealed-glass PV panels (both single- and double-layer structures) fell out completely and are more prone to developing dual flame ejections through the window than PV modules made of double-tempered glass (particularly fell out). The new openings caused by PV panel fallout altered the stable ventilation condition and induced flame ejection, thereby accelerating the growth of heat release rate and heat flux. In addition, the compartment temperature could be divided into two stages: a pre-opening phase with decelerating growth, followed by a post-opening phase caused by PV panel fallout, during which ventilation conditions were altered, resulting in higher peak temperatures compared to the control tests.

Overall, the results demonstrate that the fire performance of BIPV façades is strongly governed by the coupled effects of glass type and the presence of combustible encapsulation materials. Tempered-glass PV panels exhibit superior thermal and mechanical resistance to breakage, and falling combustible encapsulation materials may ignite lower or surrounding combustibles, thereby further promoting fire spread. In addition, the number of glass layers of the PV panels is also a significant factor. Among the tested configurations, double-glazed PV modules with tempered glass showed higher integrity and were more effective in suppressing the formation of new ventilation openings, suggesting their potential as a safer option for BIPV façade applications. To balance fire performance and mechanical safety, the fire resistance of glass and combustible encapsulation materials within the PV panels, along with the number of glass layers of the PV panels, should be considered as critical design parameters in BIPV façade engineering.

CRediT authorship contribution statement

Chengming Xiao: Writing – review & editing, Writing – original draft, Validation, Methodology, Investigation, Data curation, Conceptualization. **Rui Zhou:** Investigation, Formal analysis. **Dezhi Ran:** Investigation, Formal analysis. **Fengqi Wang:** Investigation, Formal analysis. **Haonan Chen:** Investigation, Formal analysis. **Chiara Bedon:** Writing – review & editing. **Jinhua Sun:** Writing – review & editing. **Yu Wang:** Writing – review & editing, Supervision, Project administration, Funding acquisition, Conceptualization.

Declaration of competing interest

The authors declare that they have no known competing financial interests or personal relationships that could have appeared to influence the work reported in this paper.

Acknowledgements

The authors would like to acknowledge the National Key R&D Program of China (2023YFE0116700) and National Natural Science Foundation of China (Grant No. 52176137). The Italian Ministry of Foreign Affairs and International Cooperation (CN24GR03) is also acknowledged.

Data availability

The data that has been used is confidential.

References

[1] M. Gul, Y. Kotak, T. Muneer, Review on recent trend of solar photovoltaic technology, Energy Explor. Exploit. 34 (2016) 485–526.

[2] Coherent Market Insights, Building Integrated Photovoltaics Market Analysis & Forecast: 2026-2033. Available at: https://www.coherentmarketinsights.com/industry-reports/building-integrated-photovoltaics-market.
[3] E. Saretta, P. Caputo, F. Frontini, A review study about energy renovation of building facades with BIPV in urban environment, Sustain. Cities Soc. 44 (2019) 343–355.
[4] X. Zhang, The world's first super-stage zero-carbon building put into operation in qingdao, 2025. https://en.cnesa.org/latest-news/2025/8/25/the-worlds-first-super-stage-zero-carbon-building-put-into-operation-in-qingdao.
[5] E. Reynolds, First look: inside the world's first solar-powered residential high-rise, Robb report, 2022. Available at: https://robbreport.com/shelter/new-construction/1428-brickell-worlds-first-solar-powered-high-rise-residential-tower-1234759281/.
[6] A. Brown, Austria's second-tallest tower rises with Europe-first solar facade, Construction Briefing, 2025. Available at: https://www.constructionbriefing.com/news/austrias-second-tallest-tower-rises-with-europe-first-solar-facade/8073267.article?zephr_sso_ott=BNoFIJ.
[7] L. Stamenic, E. Smiley, K. Karim, Low light conditions modelling for building integrated photovoltaic (BIPV) systems, Sol. Energy 77 (2004) 37–45.
[8] Advanced Solar Power (Hangzhou), PV facade for Swedish town. Available at: http://www.advsolarpower.com/en/index.php/case/case-info/7/194.
[9] FASEC Window Wall Group, Solar PV curtain walls application, 2024. Available at: https://www.youtube.com/watch?v=BPm1I8ZrXAE.
[10] Inhabitat, Solar ARK: world's Most stunning solar building. Available at: https://inhabitat.com/solar-ark-worlds-most-stunning-solar-building/.
[11] Senhong Glass, Glass curtain walls and facade. Available at: https://www.senhongglass.com/glass-curtain-walls-facade/.
[12] C. McGlone, Fears over solar panel safety as number of fires rises six-fold, The Independent, 2023. Available at: https://www.independent.co.uk/news/uk/home-news/solar-panel-fires-safety-fears-energy-bills-b2407950.html.
[13] D. Rogers, Brussels blaze points to growing risk of fires caused by solar panels, Global Construction Review, 2025. Available at: https://www.globalconstructionreview.com/brussels-blaze-points-to-growing-risk-of-fires-caused-by-solar-panels/.
[14] A.C.Y. Yuen, T.B.Y. Chen, A. Li, I.M. De Cachinho Cordeiro, L. Liu, H. Liu, A.L.P. Lo, Q.N. Chan, G.H. Yeoh, Evaluating the fire risk associated with cladding panels: an overview of fire incidents, policies, and future perspective in fire standards, Fire Mater. 45 (2021) 663–689.
[15] H. Chen, Y. Wang, Y. Zhang, Q. Wang, H. Zhao, G. Shao, Y. Su, J. Sun, L. He, Crack evolution process of window glass under radiant heating, Fire Mater. 41 (2017) 1016–1026.
[16] L. Li, Q. Xie, X. Cheng, H. Zhang, Cracking behavior of glazings with different thicknesses by radiant exposure, Fire Mater. 36 (2012) 264–276.
[17] Q. Wang, Y. Wang, Y. Zhang, H. Chen, J. Sun, L. He, A stochastic analysis of glass crack initiation under thermal loading, Appl. Therm. Eng. 67 (2014) 447–457.
[18] Y. Wang, Q. Wang, Y. Su, J. Sun, L. He, K. Liew, Fracture behavior of framing coated glass curtain walls under fire conditions, Fire Saf. J. 75 (2015) 45–58.
[19] R. Stølen, T. Li, T. Wingdahl, A. Steen-Hansen, Large-and small-scale fire test of a building integrated photovoltaic (BIPV) façade system, Fire Saf. J. 144 (2024) 104083.
[20] C. Chow, S. Han, X. Ni, A study on fire behaviour of combustible components of two commonly used photovoltaic panels, Fire Mater. 41 (2017) 65–83.
[21] H.-Y. Yang, X.-D. Zhou, L.-Z. Yang, T.-L. Zhang, Experimental studies on the flammability and fire hazards of photovoltaic modules, Materials 8 (2015) 4210–4225.
[22] M.-C. Despinasse, S. Krueger, First developments of a new test to evaluate the fire behavior of photovoltaic modules on roofs, Fire Saf. J. 71 (2015) 49–57.
[23] T.R. Hull, R.E. Quinn, I.G. Areri, D.A. Purser, Combustion toxicity of fire retarded EVA, Polym. Degrad. Stabil. 77 (2002) 235–242.
[24] S.S. Nair, A.M. Kulkarni, Experimental study on the flammability of photovoltaic module backsheets, Int. J. Sci. Eng. Res. 9 (2018).
[25] B. Liao, L. Yang, X. Ju, Y. Peng, Y. Gao, Experimental study on burning and toxicity hazards of a PET laminated photovoltaic panel, Sol. Energy Mater. Sol. Cell. 206 (2020) 110295.
[26] J.S. Kristensen, F.B.M. Faudzi, G. Jomaas, Experimental study of flame spread underneath photovoltaic (PV) modules, Fire Saf. J. 120 (2021) 103027.
[27] J.S. Kristensen, G. Jomaas, Experimental study of the fire behaviour on flat roof constructions with multiple photovoltaic (PV) panels, Fire Technol. 54 (2018) 1807–1828.
[28] J.S. Kristensen, B. Merci, G. Jomaas, Fire-induced reradiation underneath photovoltaic arrays on flat roofs, Fire Mater. 42 (2018) 316–323.
[29] H. Schock, Thin film photovoltaics, Appl. Surf. Sci. 92 (1996) 606–616.
[30] Y. Wang, C. Xiao, C. Bedon, Performance of photovoltaic panels with different inclinations under uniform thermal loading, Int. J. Therm. Sci. 208 (2025) 109489.
[31] Y. Wang, Experimental and numerical study of glass façade breakage behavior under fire conditions: Fire Safety Engineering, Springer, 2019.